

# Entanglement generation in microcavity polariton devices

**L. Einkemmer**

Department of Experimental Physics, University of Innsbruck, 6020 Innsbruck, Austria

**Z. Vörös**

E-mail: zvoros@uibk.ac.at

Department of Experimental Physics, University of Innsbruck, 6020 Innsbruck, Austria

**G. Weihs**

Department of Experimental Physics, University of Innsbruck, 6020 Innsbruck, Austria

**S. Portolan**

Institute of Atomic and Subatomic Physics, TU Wien, 1020 Wien, Austria

**Abstract.** Entanglement generation in microcavity exciton-polaritons is an interesting application of the peculiar properties of these half-light/half-matter quasiparticles. In this paper we theoretically investigate their luminescence dynamics and entanglement formation in single, double, and triple cavities. We derive general expressions and selection rules for polariton-polariton scattering. We evaluate a number of possible parametric scattering schemes in terms of entanglement, and identify the ones that are experimentally most promising.

## 1. Introduction

Microcavity polaritons have come to the fore of semiconductor optics research after Weisbuch et al. [1] demonstrated strong coupling of the cavity photon and the quantum well exciton. In their work, the photon in a single cavity was coupled with excitons of a quantum well located at the anti-node of the electric field. Soon afterwards, several groups demonstrated strong coupling in double [2, 3, 4, 5, 6], and triple cavities [7, 8, 9]. Beyond the fact that these structures would allow more exotic scattering scenarios, the advantage of coupled cavities is that polariton-polariton scattering can be studied on branches that are protected from the exciton reservoir, or in other context, the excitation-induced dephasing, and thus, one of the non-radiative polariton decay channels is removed. In a different context, this was already pointed out in the work of Ciuti [10], and in Pagel et al. [11].

The polariton dispersion relations (including polarization splitting) of coupled cavities were discussed in several papers, including Armitage et al. [2], Panzarini et al. [3, 4, 5], and Stanley et al. [6], while the triple cavity case was presented in Diederichs et al. [7, 8, 9]. However, all of these papers were concerned with the dispersion relations only, and, to some extent, their role in polariton-polariton scattering, but the question of scattering with other quasi-particles was not addressed. Therefore, from these works alone, it would not be clear whether a particular polariton-polariton scattering process is experimentally feasible: even if the process is allowed, the resulting polaritons could be buried in a strong background of thermal polaritons. To analyze this aspect we will extend the quantum Langevin approach introduced in [12] to double and triple cavity configurations. This approach allows us to provide quantitative predictions of noise induced by thermally scattered pump polaritons, which is expected to be the dominant source in experimentally realistic polariton devices. In addition, in the context outlined above, we are able to compare the pump-induced photoluminescence of double cavity schemes with the corresponding results for single cavity devices (which were considered in the literature before, see, for example, [13]).

In this paper, we present a detailed study of polariton scattering in multiple cavities, and identify the dominant scattering processes with the aim of finding schemes that support the generation of polarization-entangled light. The paper is organized as follows. First, starting with a simple model, we inspect the symmetry properties of polaritons in coupled and triple cavities. Based on these symmetries, we then establish some general selection rules. Following this, we derive the equations governing polariton-polariton scattering. An analytical solution and its discussion for the case of continuous-wave pumping is given in Section 5, and we measure entanglement of the produced light. The case of pulsed excitation is detailed in Section 6. Here we also compare the results to that obtained for the analytical case, and show that meaningful conclusions can be drawn from the steady state solution. We close the paper with some general remarks and a short outlook in Section 7. The technical details of our derivations are outlined in the Appendix.

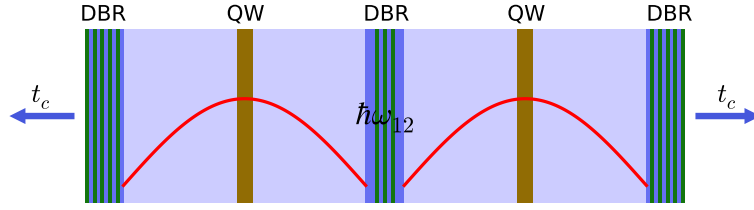


**Figure 1.** The coupled structure is shown schematically. QW and DBR are the quantum wells, and distributed Bragg reflectors, respectively, while  $t_c$  is the out-coupling of the cavity. The coupling between the two cavities is denoted by  $\hbar\omega_{12}$ .

## 2. The role of the symmetry

In the rest of the paper, we will apply the following notation: exciton, and photon states located in a particular cavity are denoted by  $|X_i\rangle$ , and  $|P_i\rangle$ , respectively, while we will use  $|p_{j\mathbf{k}}\rangle$  for a polariton on the  $j$ th branch with momentum  $\hbar\mathbf{k}$ . (The exact definition of the polariton branches will be stated below.)

The structure that we are going to study is shown schematically in figure 1; two or three microcavities are coupled through a partially reflecting mirror. All cavities have a single quantum well at their centre, which is at the location of the anti-node of the lowest-lying photon mode of the uncoupled case. For simplicity, we will not consider cavities with multiple quantum wells in this paper.

When two or three identical cavities, as described above, are coupled, the eigenmodes of the photon field are the eigenvectors of the matrices

$$\begin{pmatrix} E_{c_1} & \hbar\omega_{12} \\ \hbar\omega_{12} & E_{c_2} \end{pmatrix}$$

and

$$\begin{pmatrix} E_{c_1} & \hbar\omega_{12} & 0 \\ \hbar\omega_{12} & E_{c_2} & \hbar\omega_{23} \\ 0 & \hbar\omega_{23} & E_{c_3} \end{pmatrix},$$

respectively. Here the bare cavity energies are denoted by  $E_{c_i}$ , while  $\hbar\omega_{ij}$  is the coupling constant between cavity  $i$ , and cavity  $j$ . In standard structures,  $E_{c_i}$  is of the order of a couple of eV, while the coupling is in the meV range. The eigenvectors are denoted by  $\vec{a}^{(i)}$ , and, since these vectors belong to a symmetric matrix (see Appendices 7.2, and 7.3), we have the orthogonality condition

$$\vec{a}^{(i)} \cdot \vec{a}^{(j)} = \delta_{ij}. \quad (1)$$

For the case of equal cavity energies, and equal couplings, i.e.  $\hbar\omega_{12} = \hbar\omega_{23}$ ,  $\vec{a}^{(i)}$  can be expressed in the double cavity as

$$\vec{a}^{(1)} = \frac{1}{2}(1, 1), \quad \vec{a}^{(2)} = \frac{1}{\sqrt{2}}(1, -1)$$

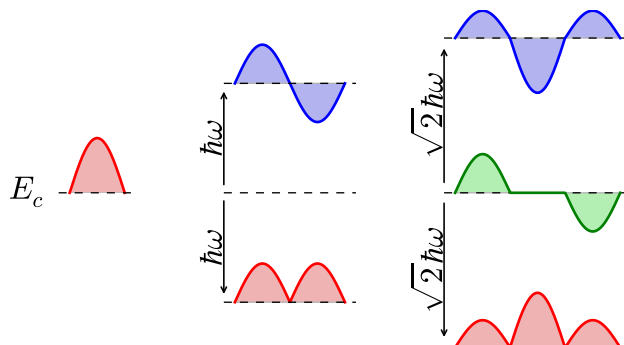


**Figure 2.** Schematic envelope of the electric field in the single (left), double (centre), and the triple cavity (right). The horizontal axis is the spatial coordinate. Also shown are the corresponding energy shifts, when all couplings between the cavities are assumed to be equal to  $\hbar\omega$ .

and in the triple cavity as

$$\begin{aligned}\vec{a}^{(1)} &= \frac{1}{2}(1, \sqrt{2}, 1), \\ \vec{a}^{(2)} &= \frac{1}{\sqrt{2}}(1, 0, -1), \\ \vec{a}^{(3)} &= \frac{1}{2}(1, -\sqrt{2}, 1).\end{aligned}$$

The resulting eigenstates are schematically shown in figure 2. Let us emphasize that, as discussed in the Appendix, the coupling exciton states have the same symmetry. What is important to note here is that in the double cavity, the photon states (and consequently, the polariton states) are either symmetric, or antisymmetric, while in the triple cavity, the two states that are shifted with respect to the single cavity are symmetric, while the unshifted state is antisymmetric. We should keep in mind, however, that the symmetric/antisymmetric designation of states is not a proper one for non-degenerate cavities, or unequal coupling constants.

As discussed in detail in the Appendix, these photon states, when coupled to the quantum well excitons, will lead to 2, 4, or 6 polariton states (branches), depending on how many cavities are coupled. The dispersion relations of the polariton states are given in figure 3.

### 2.1. Polariton-polariton scattering

For polariton-polariton processes (i.e. parametric scattering), since the scattering is mediated by the excitonic part of the particles, we can separate the intra-cavity and inter-cavity contributions, and write the transition matrix element as

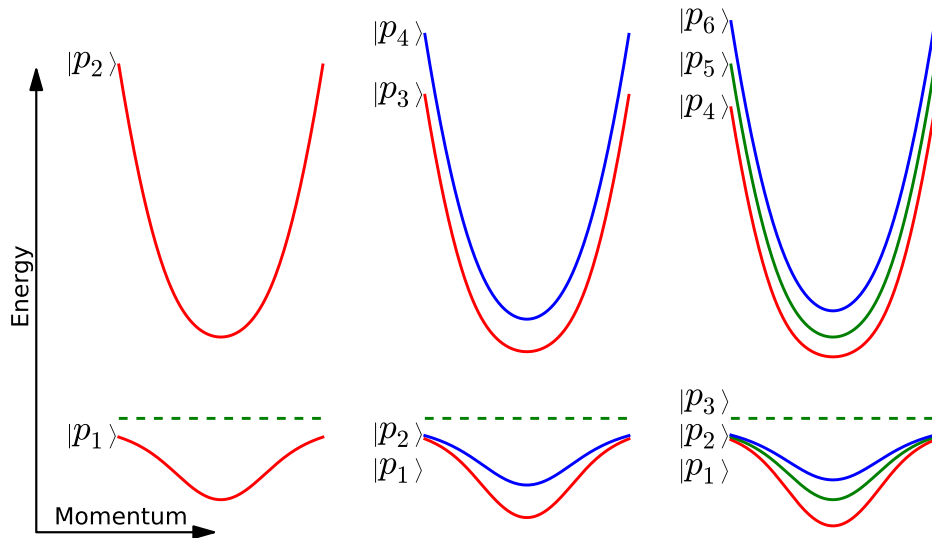


**Figure 3.** The polariton branches (solid lines) with their respective symmetries in the single (left), double (centre), and triple cavity (right). Also shown is the exciton cavity (dashed line). The Rabi splitting, i.e. the interaction strength between cavity-photons and excitons, is taken to be  $\hbar\Omega_R = 5$  meV, while the cavity splittings are  $\hbar\omega = 2$  meV. The colour of the states is taken from the underlying photon states in figure 2.

$$\langle p_i p_j | H_{\text{int}} | p_k p_l \rangle = \sum_n a_n^{(i)} a_n^{(j)} a_n^{(k)} a_n^{(l)} \langle X_1 X_1 | H_{\text{int}} | X_1 X_1 \rangle \quad (2)$$

$$+ \sum_{\substack{mn \\ m \neq n}} a_n^{(i)} a_m^{(j)} a_n^{(k)} a_m^{(l)} \langle X_1 X_2 | H_{\text{int}} | X_1 X_2 \rangle. \quad (3)$$

When contracting the sum, we assumed  $\langle X_1 X_2 | H_{\text{int}} | X_1 X_2 \rangle = \langle X_1 X_3 | H_{\text{int}} | X_1 X_3 \rangle = \langle X_2 X_3 | H_{\text{int}} | X_2 X_3 \rangle$ , i.e., that the coupling Hamiltonian is the same across cavities.

The first term in equation (3) results in a generalized parity condition for the scattering matrix element, which can be expressed concisely as

$$\begin{aligned} (\vec{a}^{(1)} * \vec{a}^{(3)}) \cdot (\vec{a}^{(2)} * \vec{a}^{(m)}) &= 0, & m \in \{1, 3\} \\ (\vec{a}^{(1)} * \vec{a}^{(2)}) \cdot (\vec{a}^{(3)} * \vec{a}^{(2)}) &\neq 0, \end{aligned}$$

using the pointwise multiplication  $*$ . Realizing that  $\vec{a}^{(1)}, \vec{a}^{(3)}$  represent symmetric branches, whereas  $\vec{a}^{(2)}$  the anti-symmetric one, a process  $|p_k p_l\rangle \rightarrow |p_i p_j\rangle$  (on the lower polariton branches) is allowed, if and only, if

$$q_k + q_l = q_i + q_j \pmod{2}, \quad (4)$$

where by  $q_k$  we denote the parity assigned to branch  $k$  which, for the three lower polariton branches, is given by

$$q_1 = 0, \quad q_2 = 1, \quad q_3 = 0.$$

For example, two polaritons from the middle branch can scatter one each to the first and third branches ( $q_2 + q_2 = q_1 + q_3 \pmod{2}$ ). We point out that equation (4) holds only for the case of degenerate cavities ( $E_{c_i} = E_{c_j}$ ), and equal couplings ( $\hbar\omega_{12} = \hbar\omega_{23}$ ).

Strictly speaking, we still have to prove that, if this condition is **not** satisfied, then the second term of the matrix element vanishes. However, it is a straightforward computation to show the desired result, i.e.

$$\sum_{\substack{mn \\ m \neq n}} a_n^{(i)} a_m^{(j)} a_n^{(k)} a_m^{(l)} = 0,$$

follows for all  $i, j, k, l$  that violate condition (4). In the double cavity case this condition is just parity conservation, as we only have one symmetric and one antisymmetric branch both below and above the exciton reservoir.

### 3. Polariton-polariton scattering amplitude in coupled cavities

In the preceding section, we showed that polaritons in coupled or triple cavities fulfil selection rules, when they scatter with either unlike particles, or other polaritons. However, these rules only tell us that certain processes are forbidden, but they do not give the scattering amplitudes. In this section, based on a general framework for polariton-polariton interaction, we derive the transition probabilities for polariton-polariton scattering.

Instead of working in the polariton basis, we start by writing down the equations of motion for the operators of the underlying photon, and exciton. When doing so, we will assume that both the cavity photons, and the excitons are confined to their respective cavities, and that an exciton can interact only with photons in the same cavity. The exciton-photon couplings are given in the Appendix in equations (17,19,22).

At least two approaches can be found in the literature for the single cavity case. First, Ciuti et al. introduced a method based on a Hamiltonian derived from scattering rates using Fermi's golden rule [14]. Their approach assumes that polaritons are bosons. Strictly speaking, this assumption is a valid approximation for low polariton densities only. Also, polariton decay is only included phenomenologically. On the other hand, this method contains the symmetries of the system more explicitly, and one can readily read off, whether a transition is allowed or not. In addition, it can be augmented to include the same quantum Langevin based phonon scattering effects, introduced by Portolan et al. [12].

Second, Portolan et al. developed a method based on the excitonic equations of motion derived from a microscopic theory of excitons in a quantum well [13, 15]. In this scheme, a phonon-induced noise term is introduced via the quantum Langevin approach. No bosonization is used and as such, the scheme is expected to more closely match experimental data. Thus, in this section, we will extend the approach by Portolan et al. to the double and triple cavity case.

In a single cavity, the equations governing the time evolution of the photon,  $a_{\mathbf{k}}$ , and exciton,  $b_{\mathbf{k}}$ , annihilation operators can be written as (see [13])

$$\frac{d}{dt}a_{\mathbf{k}} = -i(\omega_{\mathbf{k}}^c + it_c) a_{\mathbf{k}} + i\Omega_R b_{\mathbf{k}} \quad (5)$$

$$\frac{d}{dt}b_{\mathbf{k}} = -i\omega_{\mathbf{k}}^x b_{\mathbf{k}} + s_{\mathbf{k}} + i\Omega_R a_{\mathbf{k}} - \frac{i}{\hbar} R_{\mathbf{k}}^{\text{NL}} \quad (6)$$

The term  $s_{\mathbf{k}}$  only shifts the energy of the exciton. We did not include excitonic losses, for they are negligible in comparison with the transmission coefficient  $t_c$ , which denotes the leakage of photons out of the cavity. Here  $\hbar\omega_{\mathbf{k}}^c$ , and  $\hbar\omega_{\mathbf{k}}^x$  are the cavity and exciton energies at wavevector  $\mathbf{k}$ ,  $\hbar\Omega_R$  is the Rabi splitting, and  $R_{\mathbf{k}}^{\text{NL}}$  describes the non-linear exciton-exciton interaction, and can be expressed as

$$\begin{aligned} R_{\mathbf{k}}^{\text{NL}} &= R_{\mathbf{k}}^{\text{xx}} + R_{\mathbf{k}}^{\text{sat}} \\ R_{\mathbf{k}}^{\text{xx}} &= V_{\text{xx}} \sum_{\mathbf{k}_1 \mathbf{k}_2} b_{\mathbf{k}_1 + \mathbf{k}_2 - \mathbf{k}}^\dagger b_{\mathbf{k}_1} b_{\mathbf{k}_2} \\ R_{\mathbf{k}}^{\text{sat}} &= \frac{V}{n_{\text{sat}}} \sum_{\mathbf{k}_1 \mathbf{k}_2} b_{\mathbf{k}_1 + \mathbf{k}_2 - \mathbf{k}}^\dagger b_{\mathbf{k}_1} a_{\mathbf{k}_2}. \end{aligned}$$

In the equations above,  $V_{\text{xx}}$  is the exciton-exciton interaction potential, which can be approximated as a momentum-independent constant,  $V_{xx} = 6e^2/(\pi\epsilon\lambda_x)$ , where  $\lambda_x$  is the exciton Bohr radius,  $\epsilon$  is the dielectric constant, and  $e$  is the electron charge.  $n_{\text{sat}}$  denotes the exciton saturation density with the value  $n_{\text{sat}} = 7/(16\pi\lambda_x^2)$  [14]. Using equation (18), and denoting the polariton annihilation operator by  $P_{i\mathbf{k}}$ , we can write down the equations of motion in the polariton basis, and they take on the form

$$\frac{d}{dt}P_{1\mathbf{k}} = -i\omega_{1\mathbf{k}}P_{1\mathbf{k}} + \tilde{E}_{1\mathbf{k}}^{\text{in}} - i\tilde{R}_{1\mathbf{k}}^{\text{NL}} \quad (7)$$

$$\frac{d}{dt}P_{2\mathbf{k}} = -i\omega_{2\mathbf{k}}P_{2\mathbf{k}} + \tilde{E}_{2\mathbf{k}}^{\text{in}} - i\tilde{R}_{2\mathbf{k}}^{\text{NL}}, \quad (8)$$

with

$$\tilde{R}_{i\mathbf{k}}^{\text{NL}} = c_{i\mathbf{k}} R_{\mathbf{k}}^{\text{NL}}, \quad \tilde{E}_{i\mathbf{k}}^{\text{in}} = (-1)^i c_{3-i\mathbf{k}} t_c E_{\mathbf{k}}^{\text{in}}.$$

The interaction term,  $R_{\mathbf{k}}^{\text{NL}}$ , in the polariton basis is given by

$$\begin{aligned} R_{\mathbf{k}}^{\text{xx}} &= -V_{\text{xx}} \sum_{\mathbf{k}_1 \mathbf{k}_2 j_1 j_2} (-1)^{j+j_1+j_2} c_{j\mathbf{k}_1 + \mathbf{k}_2 - \mathbf{k}} c_{j_1 \mathbf{k}_1} c_{j_2 \mathbf{k}_2} p_{j\mathbf{k}_1 + \mathbf{k}_2 - \mathbf{k}}^\dagger p_{j_1 \mathbf{k}_1} p_{j_2 \mathbf{k}_2} \\ R_{\mathbf{k}}^{\text{sat}} &= \frac{V}{n_{\text{sat}}} \sum_{\mathbf{k}_1 \mathbf{k}_2 j_1 j_2} (-1)^{j+j_1} c_{j\mathbf{k}_1 + \mathbf{k}_2 - \mathbf{k}} c_{j_1 \mathbf{k}_1} c_{3-j_2 \mathbf{k}_2} p_{j\mathbf{k}_1 + \mathbf{k}_2 - \mathbf{k}}^\dagger p_{j_1 \mathbf{k}_1} p_{j_2 \mathbf{k}_2} \end{aligned}$$

where the branch indices are denoted by  $j, j_1, j_2$ .

The equations of motion in the general case can readily be written down, if we notice that a photon and an exciton are coupled only, if they are located in the same cavity, and that photons in adjacent cavities are coupled by tunnelling. We denote the energy associated with cavity-cavity coupling by  $\hbar\omega_{jl}$ . With this extra term, equations (5-6) become

$$\frac{d}{dt}a_{\mathbf{k}}^j = -i\left(\omega_{\mathbf{k}}^{c_j} + it_j\right)a_{\mathbf{k}}^j + i\sum_{l \neq j}\omega_{jl}a_{\mathbf{k}}^l + i\Omega_j b_{\mathbf{k}}^j \quad (9)$$

$$\frac{d}{dt}b_{\mathbf{k}}^j = -i\omega_{\mathbf{k}}^{x_j}b_{\mathbf{k}}^j + s_{\mathbf{k}} + i\Omega_j a_{\mathbf{k}}^j - \frac{i}{\hbar}R_{\mathbf{k}}^{\text{NL},j} . \quad (10)$$

We can then derive the appropriate expressions for  $R_{\mathbf{k}}^{\text{xx},i}$  and  $R_{\mathbf{k}}^{\text{sat},i}$ , where  $i$  denotes the cavity index. For the sake of brevity we give the result, for the double cavity case, in Appendix 7.4.

Similar (but more complicated) expressions hold for the case of the triple cavity. Their derivation is straightforward, but quite tedious, thus, we skip it here.

Once we have the equations of motion in the polariton basis, we can study any parametric scattering scheme by simply fixing the wave vectors, and the branch indices of the pumps, the signal, and the idler. These results are used to derive the coupling coefficients in the next section.

#### 4. Parametric scattering schemes

Before presenting the numerical results, it is instructive to investigate the possible parametric processes in a single, double or triple cavity. In what follows, in order to simplify references to the various scattering schemes, we introduce the notation  $ij \xrightarrow{s,d,t} kl$ , where  $ij$  stand for the branch indices of the two pump polaritons, while  $kl$  are the branch indices of the signal-idler pair polaritons. Finally,  $s, d$ , and  $t$  designate the cavity configuration, i.e., whether we are dealing with a single, double, or triple cavity. For example,  $22 \xrightarrow{s} 12$  would denote the single-cavity process that takes two pump polaritons from the second (upper) polaritons branch to the first (lower) and second polariton branches. This process would correspond to the scheme proposed by C. Ciuti [10]. We begin our discussion with the case of the single cavity.

##### 4.1. Parametric scattering in a single cavity

In this case, we have two polariton branches, and two input polaritons that we have to distribute on them. The branch-entanglement scheme of Ciuti [10], or any other scheme that has at least one pump on the upper branch, suffers from the above-mentioned problem of signal polaritons' leaking to the exciton reservoir. This can only be avoided, if both pump polaritons are on the lowest branch. Such a scheme was proposed by Portolan et al. [16]. We will denote this scheme by  $11 \xrightarrow{s} 11$ . It has already been



published in the cited work, therefore, we include it only for the sake of comparison with other schemes.

#### 4.2. Parametric scattering in a double cavity

As we have already pointed out, we are interested in scattering on the lower branches. Therefore, we have to distribute the two input, and two output polaritons on the two branches in such a way that both energy and momentum are conserved, and the parity conservation rules discussed in Section 2 are satisfied. Keeping these constraints in mind, the processes shown in figure 4 are allowed. We note here that the entanglement-generating scheme of Ciuti [10], in which the two pump polaritons are at  $k = 0$ , and the signal-idler pair is on two different branches, cannot be realized on the two lower polariton branches, because it would violate the the parity conservation rule. We do not include the intra-branch magic angle scattering [17, 18], and the scheme similar to  $11 \xrightarrow{s} 11$  for the following reasons: in the magic angle scattering, the signal and idler are at different energies, and this leads to both distinguishability, and highly different decay times, therefore, it is not a good candidate for entanglement generation, while the original scheme of Portolan et al. do not qualitatively differ in the single or double cavity cases.

However, due to the modified structure of the lower polariton branches we can implement the scattering processes illustrated in figure 4.

#### 4.3. Parametric scattering in a triple cavity

The case of the triple cavity is similar to that of the double cavity, i.e., for any two of the three lower polariton branches,  $11 \xrightarrow{d} 22$ ,  $22 \xrightarrow{d} 11$ , and  $12 \xrightarrow{d} 12$  in figure 4 would still be allowed, but in addition, we would also have the possibility of two polaritons scattering from the second branch to the first and third branch,  $22 \xrightarrow{t} 13$ , or the reverse process,  $(13 \xrightarrow{t} 22)$ , as shown in figure 4. Due to energy conservation, this latter process has to be vertical, if  $\hbar\omega_{12} = \hbar\omega_{23}$ , i.e., both the pump polaritons and the signal-idler pair are located at  $k = 0$ .

## 5. Analytical modelling

In order to develop the intuition for the dynamics in polariton scattering, we start by considering a very simple model characterized only by three parameters, the decay width  $\Gamma$  (which is mainly determined by the excitonic and photonic linewidths), the dimensionless noise background  $n$  (In this simple model the background noise includes detector noise, pump-induced photoluminescence due to the finite temperature, etc.), and  $\tilde{\Delta}$ , which combines the pump and coupling strength. For the noise is an external parameter, it is clear that this model will not be able to distinguish between the merits of different pump schemes. We will tackle this question in Section 6.

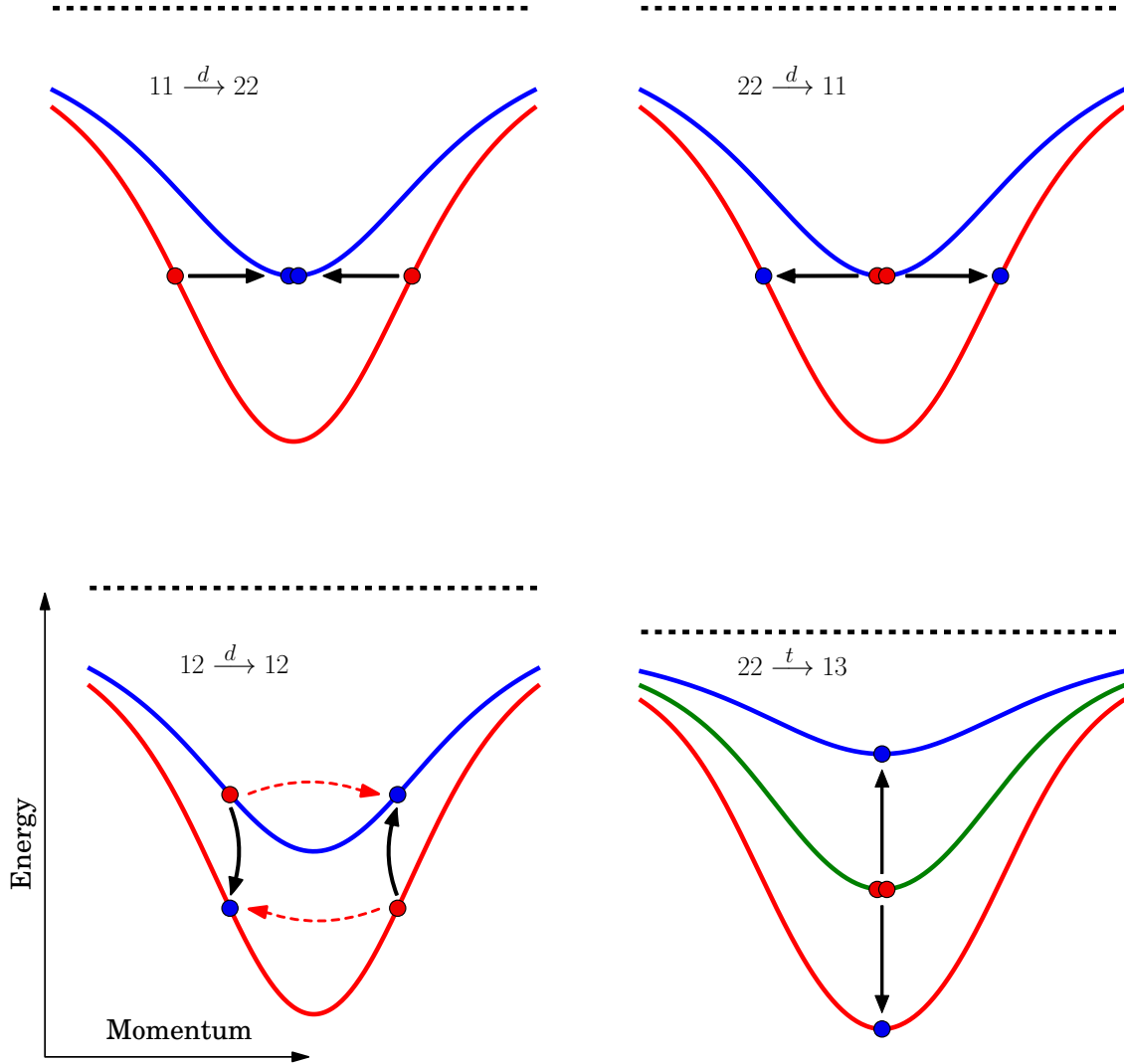


**Figure 4.** Allowed parametric scattering in a double cavity. Pump polaritons are denoted by red dots, while the signal-idler pair by blue dots. The dashed line is the exciton dispersion. The designation of the scattering processes is explained in the text.

Once the signal-idler states are fixed, the general equations of motion (7,8) decouple with respect to the momentum degree of freedom and yield a pair of two differential equations, one for the signal,  $P_s$ , and the other for the idler,  $P_i^\dagger$  [13]. The coupled two-mode system of equation reads

$$\frac{d}{dt}P_s = -i\left(\omega_s - i\frac{\Gamma_s}{2}\right)P_s - ig\mathcal{P}_1\mathcal{P}_2P_i^\dagger + \mathcal{F}_s, \quad (11)$$

$$\frac{d}{dt}P_i^\dagger = i\left(\omega_i + i\frac{\Gamma_i}{2}\right)P_i^\dagger + ig^*\mathcal{P}_1^*\mathcal{P}_2^*P_s + \mathcal{F}_i^\dagger, \quad (12)$$

where  $\mathcal{P}_{1,2}$  are the expectation values corresponding to the pump operators  $P_{1,2}$ , and the

background noise  $n$  enters through the time-dependent Langevin noise operators  $\mathcal{F}_s$  and  $\mathcal{F}_i$ . Under continuous driving conditions the effect of noise is fully determined by the stationary correlators  $\langle \mathcal{F}_m^\dagger(t) \mathcal{F}_m(t') \rangle = \Gamma n \delta(t-t')$  and  $\langle \mathcal{F}_m(t) \mathcal{F}_m^\dagger(t') \rangle = \Gamma(n+1) \delta(t-t')$ , where  $\Gamma$  is the total polariton decay rate of the particular mode, and  $m = i, s$ . Note that  $n$  is a function of the temperature, as well as of the cavity under consideration. This parameter can be determined by solving a Boltzmann-type equation [13].

The equations of motion of this model can be solved analytically in the steady state [12], and the signal population  $N_s(t)$  can be expressed as

$$N_s(t) = |c_1^s(0, t)|^2 N_s(0) + |c_2^s(0, t)|^2 (N_i(0) + 1) \\ + \Gamma n \int_0^t d\tau |c_1^s(\tau, t)|^2 + \Gamma(n+1) \int_0^t d\tau |c_2^s(\tau, t)|^2$$

while the correlators take on the form

$$\langle P_s^\dagger(t_1) P_i^\dagger(t_2) \rangle = c_1^s(0, t_1)^* c_2^i(0, t_2) N_s(0) + c_2^s(0, t_1)^* c_1^i(0, t_2) (N_i(0) + 1) \\ + \Gamma n \int_0^{\min(t_1, t_2)} du c_1^s(u, t_1) c_2^i(u, t_2)^* \\ + \Gamma(n+1) \int_0^{\min(t_1, t_2)} du c_2^s(u, t_1) c_1^i(u, t_2)^*,$$

where

$$c_1^{s,i}(t_1, t_2) = e^{(-i\omega_{s,i} - \frac{\Gamma}{2})(t_2 - t_1)} \cosh(\tilde{\Delta}(t_2 - t_1)) \\ c_2^{s,i}(t_1, t_2) = e^{(-i\omega_{s,i} - \frac{\Gamma}{2})(t_2 - t_1)} \sinh(\tilde{\Delta}(t_2 - t_1)).$$

The pump, as well as, the coupling strength enter these equations via the  $\tilde{\Delta}$  parameter which is given by

$$\tilde{\Delta} = g\mathcal{P}_1\mathcal{P}_2,$$

where  $\mathcal{P}_1, \mathcal{P}_2$  are constant in time.

Since all the information of the present model is contained in the three parameters  $\Gamma$ ,  $n$  and  $\tilde{\Delta}$ , we can apply it equally well to the single and double cavity case. We will see in the subsequent discussion that the double cavity has some advantages over the single cavity, if phonon-induced photoluminescence is considered.

We proceed by writing out the explicit expression for the population and correlation in the steady state (assuming that  $\Gamma > 2\tilde{\Delta}$ )

$$N_s(t \rightarrow \infty) = N_i(t \rightarrow \infty) = \frac{n\Gamma^2 + 2\tilde{\Delta}^2}{\Gamma^2 - 4\tilde{\Delta}^2} \\ \langle P_s^\dagger(t \rightarrow \infty) P_i^\dagger(t \rightarrow \infty) \rangle \langle P_s(t \rightarrow \infty) P_i(t \rightarrow \infty) \rangle = \left( \frac{(1+2n)\Gamma\tilde{\Delta}}{\Gamma^2 - 4\tilde{\Delta}^2} \right)^2.$$

In order to tomographically reconstruct the populations and correlations, we have to write down the two-particle density matrix [19]. By denoting the relative phase of the two pump beams by  $\Theta$ , after some simple, but tedious algebra, the density matrix can be written as (we have renormalized  $\tilde{\Delta}$  by  $\Gamma$  such that the two dimensionless quantities  $\Delta = \tilde{\Delta}/\Gamma$  and  $n$  remain as the only parameters)

$$\rho = \frac{1}{16\Delta^4 + 2(4n(n+3) + 1)\Delta^2 + 4n^2} \quad (13)$$

$$\cdot \begin{bmatrix} \rho_{11} & 0 & 0 & e^{-4i\theta}(2n\Delta + \Delta)^2 \\ 0 & (2\Delta^2 + n)^2 & 0 & 0 \\ 0 & 0 & (2\Delta^2 + n)^2 & 0 \\ e^{4i\theta}(2n\Delta + \Delta)^2 & 0 & 0 & \rho_{11} \end{bmatrix}, \quad (14)$$

where  $\rho_{11} = 4\Delta^4 + (4n(n+2) + 1)\Delta^2 + n^2$ . This expression for the density matrix allows us to calculate the entanglement of formation (EOF) with respect to the polarization degree of freedom as a function of both the (uniform) noise background, and the pump intensities [20, 21]. The EOF has a direct operational meaning as the minimum amount of information needed to form the entangled state under investigation out of uncorrelated ones.

The result is plotted in figure 5, while an approximate, but physically more transparent expression is given in the Appendix, in 7.5.

It is no surprise that the higher the noise background, the harder we have to pump, and that the maximal achievable entanglement of formation decreases with increasing noise background. It should, however, be noted that even though photoluminescence (and thus temperature effects) can be included in this model in the noise background  $n$ , this is insufficient to evaluate the merit of different pump schemes, as we are not able to ascertain the dependence of  $n$  on the temperature. In any instance, the maximum achievable entanglement is already significantly reduced not only for moderate values of  $n$  but also for moderate values of the pump intensity. In addition, the pump intensity needed to achieve the maximal entanglement of formation for a fixed noise background is not a linear function of  $n$ .

For a realistic system, temperature effects and pump induced photoluminescence, in addition, decrease the achievable entanglement. This is the topic of the next section.

## 6. Numerical simulations

In the previous section, we saw that an analytical model cannot capture all details of the polariton-polariton scattering problem at hand. For a fuller understanding, we have to resort to the numerical solutions of equations (9-10).

By applying the procedure outlined in section 3 (i.e. fixing the signal and idler as well as the pump configuration) and promoting the two remaining equations to the

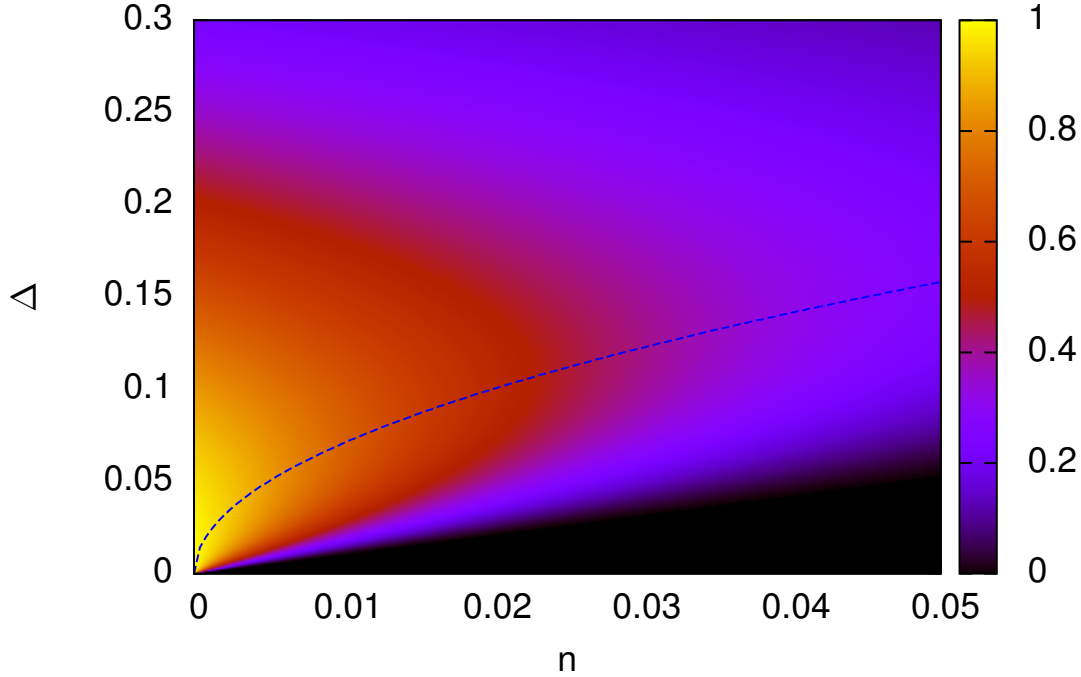


**Figure 5.** The entanglement of formation as a function of  $\Delta$  and the noise background  $n$ . Also shown is the contour of the maximum achievable entanglement. The black region ( $\Delta < n$ ) corresponds to zero entanglement of formation.

desired Heisenberg-Langevin equations, we get

$$\frac{d}{dt}P_{j_s\mathbf{k}_s} = -i\tilde{\omega}_{\mathbf{k}}P_{j_s\mathbf{k}_s} + g_{\mathbf{k}}\mathcal{P}_{\mathbf{k}_{p_1}}\mathcal{P}_{\mathbf{k}_{p_2}}P_{j_i\mathbf{k}_i} + \mathcal{F}_{P_s} \quad (15)$$

$$\frac{d}{dt}P_{j_i\mathbf{k}_i}^\dagger = i\tilde{\omega}_{\mathbf{k}_i}P_{j_i\mathbf{k}_i}^\dagger + g_{\mathbf{k}}^*\mathcal{P}_{\mathbf{k}_{p_1}}^*\mathcal{P}_{\mathbf{k}_{p_2}}^*P_{j_s\mathbf{k}_s} + \mathcal{F}_{P_i}^\dagger. \quad (16)$$

Here  $\mathcal{F}_{P_{s,i}}$  are Markovian noise operators [12].

We duly note that these equations are the same for Portolan's as well as Ciuti's approach. The difference manifests itself only in a different value for the coupling  $g_{\mathbf{k}}$ , as shown in Table 1.

First, we investigate the dependence of the entanglement of formation on the pump intensity. The results are shown in figure 7. Compared to the analytical model, we have set the uniform noise background to 0, and only considered pump-induced photoluminescence. Apart from this fact, the qualitative behaviour of the solutions is similar to the steady-state case. However, the pump-induced photoluminescence results in a more rapid decay as a function of the pump intensity.

Regarding the various pump schemes, especially in the region of moderate pump intensities (that are promising for entanglement generation), the  $22 \xrightarrow{d} 11$ , as well as the  $11 \xrightarrow{d} 22$  schemes are superior to both the  $11 \xrightarrow{s} 11$ , and the  $11 \xrightarrow{d} 11$  schemes, as demonstrated in Fig. 6. This behaviour is likely due to the fact that since signal and idler are located at the same wavevector the effective population for stimulated polariton

Scheme	Model	coefficient of $2V_{xx}$	coefficient of $\frac{V}{\tau_{\text{sat}}}$
$11 \xrightarrow{s} 11$	Portolan	$c_{1k}c_{1k_i}c_{1k_{p1}}c_{1k_{p2}}$	$c_{1k}c_{1k_i} \left[ c_{1k_{p1}}c_{2k_{p2}} + c_{2k_{p1}}c_{1k_{p2}} \right]$
	Ciuti	$c_{1k}c_{1k_i}c_{1k_{p1}}c_{1k_{p2}}$	$2 \left[ c_{2k_i}c_{1k} + c_{2k}c_{1k_i} \right] c_{1k_{p1}}c_{1k_{p2}} + 2c_{1k}c_{1k_i} \left[ c_{1k_{p1}}c_{2k_{p2}} + c_{2k_{p1}}c_{1k_{p2}} \right]$
$11 \xrightarrow{d} 11$	Portolan	$\frac{1}{2}c_{1k}c_{1k_i}c_{1k_{p1}}c_{1k_{p2}}$	$\frac{1}{2}c_{1k}c_{1k_i} \left[ c_{1k_{p1}}c_{2k_{p2}} + c_{1k_{p2}}c_{2k_{p1}} \right]$
	Ciuti	$\frac{1}{2}c_{1k}c_{1k_i}c_{1k_{p1}}c_{1k_{p2}}$	$c_{1k_{p1}}c_{2k_{p2}} \left[ c_{1k}c_{2k_i} + c_{2k}c_{1k_i} \right] + \left[ c_{1k_{p1}}c_{2k_{p2}} + c_{2k_{p1}}c_{1k_{p2}} \right] c_{1k}c_{1k_i}$
$11 \xrightarrow{d} 22$	Portolan	$\frac{1}{2}c_{3k}c_{3k_i}c_{1k_{p1}}c_{1k_{p2}}$	$\frac{1}{2}c_{3k}c_{3k_i} \left[ c_{1k_{p1}}c_{1k_{p2}} + c_{1k_{p2}}c_{2k_{p1}} \right]$
	Ciuti	$\frac{1}{2}c_{3k}c_{3k_i}c_{1k_{p1}}c_{1k_{p2}}$	$c_{1k_{p1}}c_{1k_{p2}} \left[ c_{3k}c_{4k_i} + c_{4k}c_{3k_i} \right] + \left[ c_{1k_{p1}}c_{2k_{p2}} + c_{2k_{p1}}c_{1k_{p2}} \right] c_{3k}c_{3k_i}$
$22 \xrightarrow{d} 11$	Portolan	$\frac{1}{2}c_{1k}c_{1k_i}c_{3k_{p1}}c_{3k_{p2}}$	$\frac{1}{2}c_{1k}c_{1k_i} \left[ c_{3k_{p1}}c_{4k_{p2}} + c_{3k_{p2}}c_{4k_{p1}} \right]$
	Ciuti	$\frac{1}{2}c_{1k}c_{1k_i}c_{3k_{p1}}c_{3k_{p2}}$	$c_{3k_{p1}}c_{3k_{p2}} \left[ c_{1k}c_{2k_i} + c_{2k}c_{1k_i} \right] + \left[ c_{3k_{p1}}c_{4k_{p2}} + c_{4k_{p1}}c_{3k_{p2}} \right] c_{1k}c_{1k_i}$

Table 1. Coupling coefficient  $g_{\mathbf{k}}$  for different schemes with respect to both models.

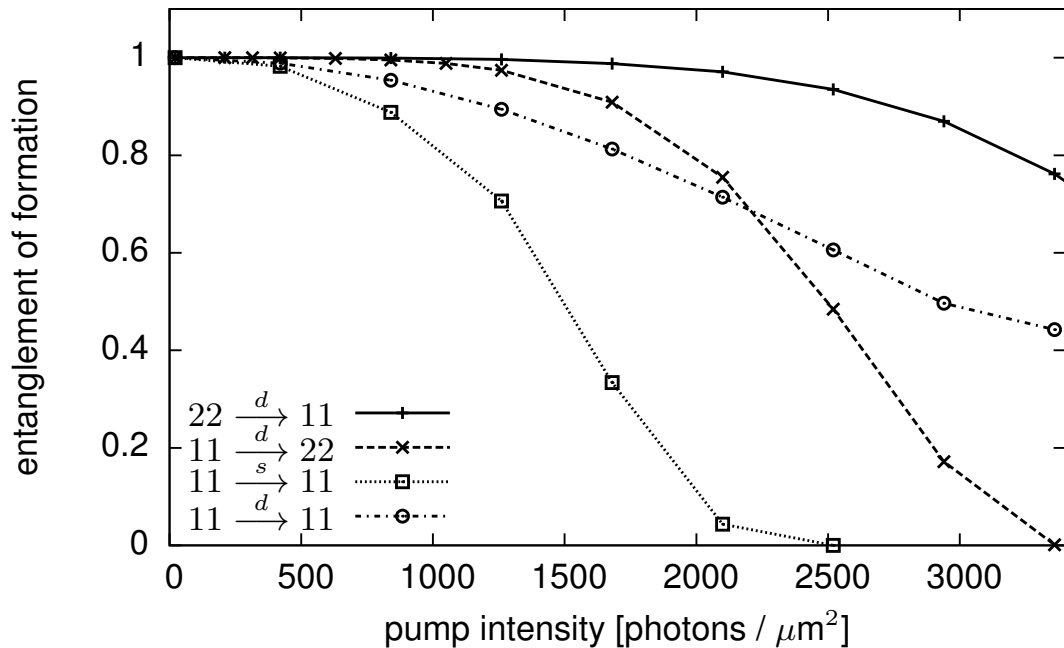


**Figure 6.** Entanglement of formation as a function of the pump intensity (in units of photons per  $\mu\text{m}^2$ ) for the  $11 \xrightarrow{s} 11$ ,  $11 \xrightarrow{d} 11$ ,  $22 \xrightarrow{s} 11$ , and  $11 \xrightarrow{d} 22$  pump schemes.

scattering is increased. The difference between the  $11 \xrightarrow{s} 11$  and  $11 \xrightarrow{d} 11$  scheme is the additional factor of  $\frac{1}{2}$  in the coupling coefficient (see Table 1), which accounts for most of the discrepancy in the entanglement of formation. In the double cavity case, the modified Hopfield coefficients contribute negligibly to  $g_{\mathbf{k}}$ .

Next, we consider the second parameter of a Gaussian pulse, the pulse width  $\tau_p$ , which is also of paramount importance, if a highly entangled state is to be achieved. This is due to the fact that there exists a unique peak close to the decay width of the cavity, more precisely at  $\tau_p \approx 0.7/\gamma$  for cavity decay width  $\gamma$ , such that the peak polariton population is maximized (see figure 7); this, in turn, has a detrimental effect on the achievable entanglement of formation. The numerical simulation shown in figure 7 exhibits a drop in the entanglement of formation in a region around  $\tau_p \approx 10$  ps, as expected from this considerations. For large  $\tau_p$  our simulation approximates the steady state case discussed in section 5.

Therefore, it is advisable to either pump with as narrow pulses as possible (in schemes where photoluminescence is a concern), or to go to the steady state case, which is only possible, if a branch protected from pump-induced photoluminescence is employed.

The time dependence of the signal polariton population can be used to highlight the difference between the models of Ciuti et al., and Portolan et al. This is shown in figure 8, where we fixed the pump wavevectors at  $\mathbf{k} = (0, 0)$  and  $\mathbf{k} = (0.9, 0.9) \mu\text{m}^{-1}$ . In addition, we set the pump intensity to  $400$  photons/ $\mu\text{m}^2$ . The width of the Gaussian pulse is chosen to be  $1$  ps. The pump configuration corresponds to the  $11 \xrightarrow{s} 11$  scheme.

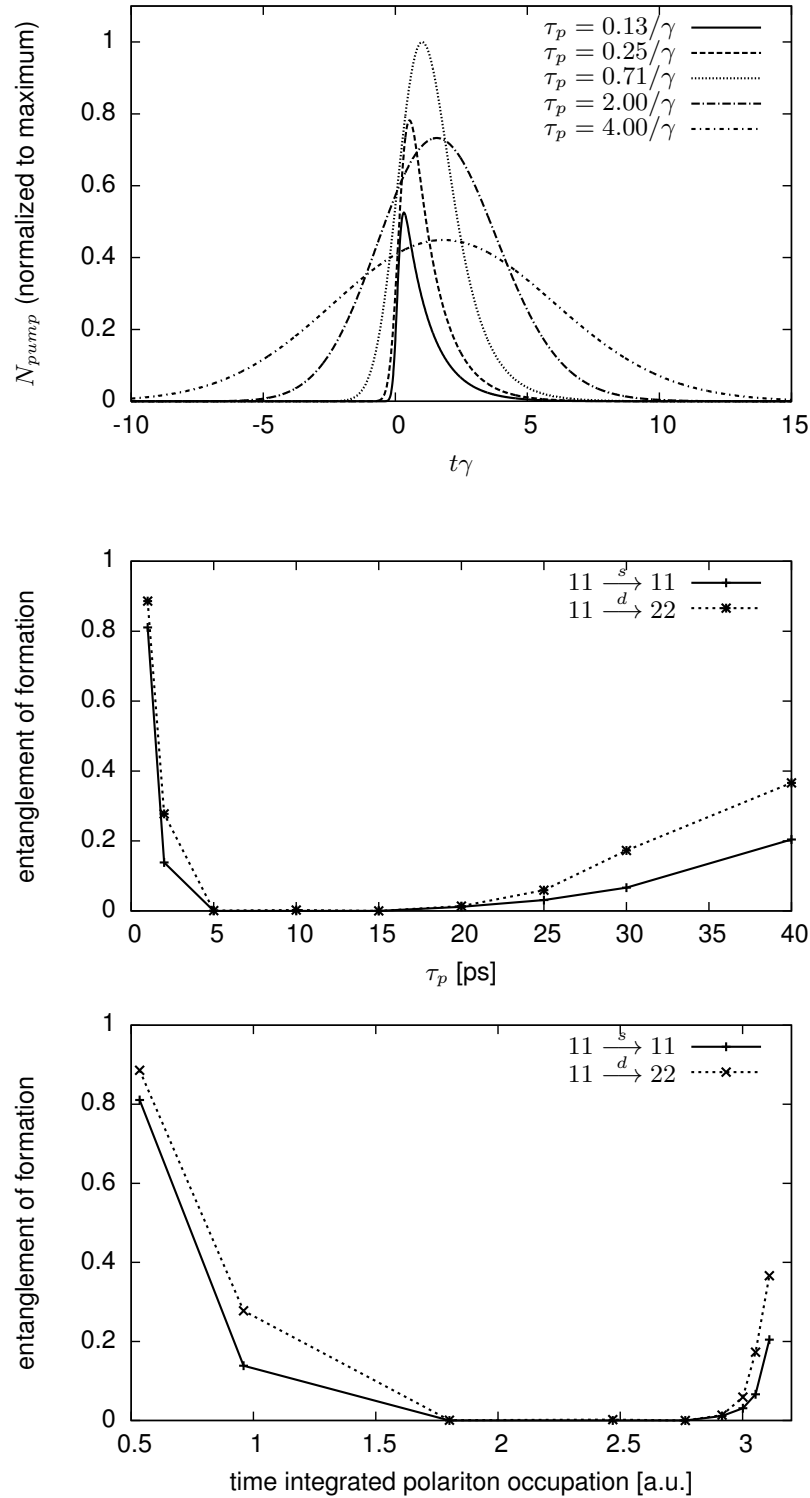


**Figure 7.** The dependence of the polariton population (top) and that of the entanglement of formation (middle) on the pulse width. The figure on the bottom is the same as the figure in the middle, with the exception that the horizontal axis is measured in the total polariton density per pulse (i.e., integrated over the duration of the excitation pulse.)



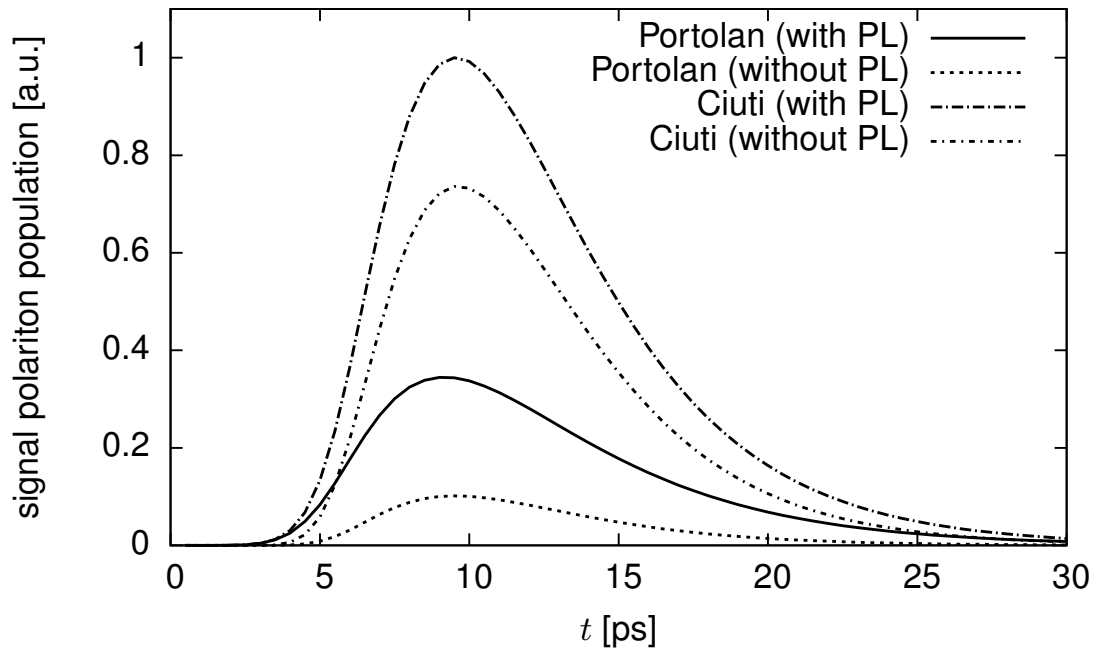


**Figure 8.** Time dependence of the signal polariton population for a pump intensity of  $400 \text{ photons}/\mu\text{m}^2$ , pulse width of 1 ps, and  $\hbar\Omega = 3 \text{ meV}$ . The model of Ciuti et al. gives higher populations than the model of Portolan et al. both with, and without background photoluminescence.

In both cases the signal population is higher when the photoluminescence is switched on. It is also clear that either with or without photoluminescence, the population is lower in the model of Portolan et al. This difference between the two models is nothing, but the consequence of the difference of the coupling coefficients, as shown in Table 1. We should note, however, that the shape of the time evolution in the two models is approximately the same, and therefore, an experimental verification of either of them would require the measurement of either absolute intensities or the investigation of the  $k$  dependence.

## 7. Conclusions

In this paper, we presented a unified treatment of polariton-polariton scattering in single, double, and triple planar microcavities, and discussed the selection rules that govern interbranch scattering. Using both a simplified analytical, and full numerical simulations of the equations of motion, we also investigated how entanglement in various scattering configurations emerges from a noisy environment caused by background processes. To model the pump-induced photoluminescence the simulations have been conducted in the framework of a quantum Langevin approach. These simulations demonstrated that the double cavity configuration possesses an advantage over single cavities, because the phonon-induced photoluminescence is somewhat suppressed. In practice, however,

additional noise sources may be present, such as resonant Rayleigh scattering. The double and triple cavity configurations allow us to choose phase-matching schemes that improve the practical separation of pump and detection beams in an experiment. In addition, we found that the entanglement of formation depends quite sensitively on the temporal width of the pump laser. This is important, because temporal selection of the detected photons is limited by the time resolution of the photodetectors. The fastest single-photon sensitive photodetectors have a time resolution of several ten picoseconds. Thus, the temporal optimization can only be done on the excitation side. Finally, we performed a quantitative comparison of two different approaches to the calculation of the scattering coefficients and we hope that with new experimental results we will soon be able to decide which approach can better model the dynamics in semiconductor microcavities.

## Acknowledgements

This work was funded in part by the European Research Council Project No. 257531, and the Canadian Institute for Advanced Research (CIFAR) through its QIP program. S.P. acknowledges support by the Austrian Science Fund (FWF) through the START grant Y 591-N16.

## Appendix

In this part of the paper, we discuss the symmetry properties of the various polariton states in single, double, and triple planar microcavities as well as give the interaction terms for the double cavity case.

### 7.1. Single cavity

In the basis of the exciton,  $|X\rangle$ , and the cavity photon,  $|P\rangle$ , the Hamiltonian of the system is given by

$$H_1 = \begin{pmatrix} E_x & \hbar\Omega \\ \hbar\Omega & E_c \end{pmatrix} \quad (17)$$

and the eigenstates are the lower and upper polaritons,

$$\begin{aligned} |p_1\rangle &= c_1 |X\rangle + c_2 |P\rangle \\ |p_2\rangle &= -c_2 |X\rangle + c_1 |P\rangle \end{aligned}$$

or in matrix form,

$$\begin{pmatrix} |p_1\rangle \\ |p_2\rangle \end{pmatrix} = \begin{pmatrix} c_1 & c_2 \\ -c_2 & c_1 \end{pmatrix} \begin{pmatrix} |X\rangle \\ |P\rangle \end{pmatrix} \quad (18)$$

The eigenvalues take on the form

$$E_j = \frac{1}{2} \left( E_c(\mathbf{k}) - E_x(\mathbf{k}) + (-1)^j \sqrt{(E_c(\mathbf{k}) - E_x(\mathbf{k}))^2 + (2\hbar\Omega)^2} \right),$$

while the Hopfield coefficients,  $c_1, c_2$ , are given by the relation

$$|c_j|^2 = \frac{1}{2} \left( 1 + (-1)^j \frac{E_c(\mathbf{k}) - E_x(\mathbf{k})}{\sqrt{(E_c(\mathbf{k}) - E_x(\mathbf{k}))^2 + (2\hbar\Omega)^2}} \right).$$

Note that  $c_1$ , and  $c_2$  represent the excitonic and photonic content of the first polariton branch, respectively, while the reverse is true for the second branch.

## 7.2. Double cavity

In the basis of the two excitons, and two photons located in their respective cavities, the Hamiltonian takes on the form

$$H_2 = \begin{pmatrix} E_{x_1} & \hbar\Omega_1 & 0 & 0 \\ \hbar\Omega_1 & E_{c_1} & 0 & -\hbar\omega_{12} \\ 0 & 0 & E_{x_2} & \hbar\Omega_2 \\ 0 & -\hbar\omega_{12} & \hbar\Omega_2 & E_{c_2} \end{pmatrix} \quad (19)$$

(Note that the ordering of the basis states is  $|X_1\rangle - |P_1\rangle - |X_2\rangle - |P_2\rangle$ .) This Hamiltonian can be made block-diagonal by transformation of the unitary matrix

$$U_2 = U_2^{-1} = \frac{1}{\sqrt{2}} \begin{pmatrix} 1 & 0 & 1 & 0 \\ 0 & 1 & 0 & 1 \\ 1 & 0 & -1 & 0 \\ 0 & 1 & 0 & -1 \end{pmatrix} \quad (20)$$

i.e., if we use the symmetric-antisymmetric combinations of the two exciton, and photon states. In the new basis, the Hamiltonian reads as

$$\tilde{H}_2 = U_2 H_2 U_2^{-1} = \begin{pmatrix} E_{x_1}(\mathbf{k}) & \hbar\Omega_1 & 0 & 0 \\ \hbar\Omega_1 & E_{c_1}(\mathbf{k}) - \hbar\omega_{12} & 0 & 0 \\ 0 & 0 & E_{x_2}(\mathbf{k}) & \hbar\Omega_2 \\ 0 & 0 & \hbar\Omega_2 & E_{c_2}(\mathbf{k}) + \hbar\omega_{12} \end{pmatrix} \quad (21)$$

and one can readily read off the new eigenstates, which are nothing, but the eigenstates of the single-cavity Hamiltonian in equation (17), with a shift in the cavity energies. If we assume, moreover, that  $\Omega = \Omega_1 = \Omega_2$ ,  $E_x = E_{x_1} = E_{x_2}$ ,  $\omega = \omega_{12}$ , and  $E_c = E_{c_1} = E_{c_2}$ , i.e., that the unperturbed exciton and cavity energies are degenerate, and that the Rabi splitting does not depend on the parity of the states, then the eigenvalues of equation (21) take on the particularly simple form

$$E_j = \frac{E_c(\mathbf{k}) + (-1)^j \hbar\omega + E_x(\mathbf{k}) + (-1)^{\lfloor (j+1)/2 \rfloor} \sqrt{(E_c(\mathbf{k}) + (-1)^j \hbar\omega - E_x(\mathbf{k}))^2 + (2\hbar\Omega)^2}}{2}$$

with the four eigenvectors

$$\begin{pmatrix} |p_1\rangle \\ |p_2\rangle \\ |p_3\rangle \\ |p_4\rangle \end{pmatrix} = \frac{1}{\sqrt{2}} \begin{pmatrix} c_1 & c_2 & c_1 & c_2 \\ c_3 & c_4 & -c_3 & -c_4 \\ -c_2 & c_1 & -c_2 & -c_1 \\ -c_4 & c_3 & c_4 & -c_3 \end{pmatrix} \begin{pmatrix} |X_1\rangle \\ |P_1\rangle \\ |X_2\rangle \\ |P_2\rangle \end{pmatrix}$$

where the Hopfield coefficients are given by

$$|c_j|^2 = \frac{1}{2} \left( 1 + (-1)^{\lfloor (j+1)/2 \rfloor} \frac{E_c(\mathbf{k}) + (-1)^j \hbar\omega - E_x(\mathbf{k})}{\sqrt{(E_c(\mathbf{k}) + (-1)^j \hbar\omega - E_x(\mathbf{k}))^2 + (2\hbar\Omega)^2}} \right)$$

### 7.3. Triple cavity

Ordering the states as  $|X_1\rangle - |P_1\rangle - |X_2\rangle - |P_2\rangle - |X_3\rangle - |P_3\rangle$  in the basis of the three excitons, and three photons located in the three cavities, the Hamiltonian reads as

$$H_3 = \begin{pmatrix} E_{x_1}(\mathbf{k}) & \hbar\Omega_1 & 0 & 0 & 0 & 0 \\ \hbar\Omega_1 & E_{c_1}(\mathbf{k}) & 0 & -\hbar\omega_{12} & 0 & 0 \\ 0 & 0 & E_{x_2}(\mathbf{k}) & \hbar\Omega_2 & 0 & 0 \\ 0 & -\hbar\omega_{12} & \hbar\Omega_2 & E_{c_2}(\mathbf{k}) & 0 & -\hbar\omega_{23} \\ 0 & 0 & 0 & 0 & E_{x_3} & \hbar\Omega_3 \\ 0 & 0 & 0 & -\hbar\omega_{23} & \hbar\Omega_3 & E_{c_3} \end{pmatrix} \quad (22)$$

Again, with the simplifying assumption  $\Omega = \Omega_1 = \Omega_2 = \Omega_3$ ,  $E_x = E_{x_1} = E_{x_2} = E_{x_3}$ ,  $\omega = \omega_{12} = \omega_{23}$ , and  $E_c = E_{c_1} = E_{c_2} = E_{c_3}$ , the transformation matrix

$$U_3 = \frac{1}{\sqrt{2}} \begin{pmatrix} 1 & 0 & 0 & 0 & -1 & 0 \\ 0 & 1 & 0 & 0 & 0 & -1 \\ \frac{1}{\sqrt{2}} & 0 & 1 & 0 & \frac{1}{\sqrt{2}} & 0 \\ 0 & \frac{1}{\sqrt{2}} & 0 & 1 & 0 & \frac{1}{\sqrt{2}} \\ \frac{1}{\sqrt{2}} & 0 & -1 & 0 & \frac{1}{\sqrt{2}} & 0 \\ 0 & \frac{1}{\sqrt{2}} & 0 & -1 & 0 & \frac{1}{\sqrt{2}} \end{pmatrix} \quad (23)$$

brings  $H_3$  into a block-diagonal form, and we get

$$\tilde{H}_3 = U_3 H_3 U_3^{-1} = \begin{pmatrix} E_x & \hbar\Omega & 0 & 0 & 0 & 0 \\ \hbar\Omega & E_c - \sqrt{2}\hbar\omega & 0 & 0 & 0 & 0 \\ 0 & 0 & E_x & \hbar\Omega & 0 & 0 \\ 0 & 0 & \hbar\Omega & E_c & 0 & 0 \\ 0 & 0 & 0 & 0 & E_x & \hbar\Omega \\ 0 & 0 & 0 & 0 & \hbar\Omega & E_c + \sqrt{2}\hbar\omega \end{pmatrix} \quad (24)$$

with the eigenvalues

$$E_j = \frac{E_c(\mathbf{k}) - 2\hbar\omega \cos\left(j\frac{\pi}{4}\right) + E_x(\mathbf{k})}{2} + \frac{(-1)^{\lfloor \frac{j+2}{3} \rfloor} \sqrt{(E_c(\mathbf{k}) - 2\hbar\omega \cos\left(j\frac{\pi}{4}\right) - E_x(\mathbf{k}))^2 + (2\hbar\Omega)^2}}{2}$$

The polariton eigenstates are

$$\begin{pmatrix} |p_1\rangle \\ |p_2\rangle \\ |p_3\rangle \\ |p_4\rangle \\ |p_5\rangle \\ |p_6\rangle \end{pmatrix} = \begin{pmatrix} \frac{c_1}{\sqrt{2}} & \frac{c_2}{\sqrt{2}} & 0 & 0 & -\frac{c_1}{\sqrt{2}} & -\frac{c_2}{\sqrt{2}} \\ -\frac{c_2}{\sqrt{2}} & \frac{c_1}{\sqrt{2}} & 0 & 0 & \frac{c_2}{\sqrt{2}} & -\frac{c_1}{\sqrt{2}} \\ \frac{c_3}{2} & \frac{c_4}{2} & \frac{c_3}{\sqrt{2}} & \frac{c_4}{\sqrt{2}} & \frac{c_3}{2} & \frac{c_4}{2} \\ -\frac{c_4}{2} & \frac{c_3}{2} & -\frac{c_4}{\sqrt{2}} & \frac{c_3}{\sqrt{2}} & -\frac{c_4}{2} & \frac{c_3}{2} \\ \frac{c_5}{2} & \frac{c_6}{2} & -\frac{c_5}{\sqrt{2}} & -\frac{c_6}{\sqrt{2}} & \frac{c_5}{2} & \frac{c_6}{2} \\ -\frac{c_6}{2} & \frac{c_5}{2} & \frac{c_6}{\sqrt{2}} & -\frac{c_5}{\sqrt{2}} & -\frac{c_6}{2} & \frac{c_5}{2} \end{pmatrix} \begin{pmatrix} |X_1\rangle \\ |P_1\rangle \\ |X_2\rangle \\ |P_2\rangle \\ |X_3\rangle \\ |P_3\rangle \end{pmatrix}$$

where we have simplified the matrix by noting that  $c_1^2 + c_2^2 = c_3^2 + c_4^2 = c_5^2 + c_6^2 = 1$ .  $c_j$  are the Hopfield coefficients of the three block-diagonals in equation (23), and are given by

$$|c_j|^2 = \frac{1}{2} \left( 1 + (-1)^{\lfloor \frac{j+2}{3} \rfloor} \frac{E_c(\mathbf{k}) - 2\hbar\omega \cos\left(j\frac{\pi}{4}\right) - E_x(\mathbf{k})}{\sqrt{(E_c(\mathbf{k}) - 2\hbar\omega \cos\left(j\frac{\pi}{4}\right) - E_x(\mathbf{k}))^2 + (2\hbar\Omega)^2}} \right).$$

By applying the transformation, we changed the description of the problem from the basis of excitons and photons located in their respective cavity to the basis of the totally antisymmetric,  $|X_{as}\rangle = \frac{1}{\sqrt{2}}(|X_1\rangle - |X_3\rangle)$ , and totally symmetric  $|X_{s1}\rangle = \frac{1}{2}|X_1\rangle + \frac{1}{\sqrt{2}}|X_2\rangle + \frac{1}{2}|X_3\rangle$ ,  $|X_{s2}\rangle = \frac{1}{2}|X_1\rangle - \frac{1}{\sqrt{2}}|X_2\rangle + \frac{1}{2}|X_3\rangle$  wavefunctions. (Similar expressions apply to the photon states.)



## 7.4. The interaction terms in the polariton basis

$$\begin{aligned}
R_{\mathbf{k}}^{\text{xx},1} &= V_{\text{xx}} \sum_{\mathbf{k}_1, \mathbf{k}_2} B_{1\mathbf{k}_1 + \mathbf{k}_2 - \mathbf{k}}^\dagger B_{1\mathbf{k}_1} B_{1\mathbf{k}_2} \\
&= \frac{V_{\text{xx}}}{2\sqrt{2}} \sum_{\mathbf{k}_1, \mathbf{k}_2} \left\{ \left( c_{1\mathbf{k}_1 + \mathbf{k}_2 - \mathbf{k}} p_{1\mathbf{k}_1 + \mathbf{k}_2 - \mathbf{k}}^\dagger + c_{3\mathbf{k}_1 + \mathbf{k}_2 - \mathbf{k}} p_{2\mathbf{k}_1 + \mathbf{k}_2 - \mathbf{k}}^\dagger - c_{2\mathbf{k}_1 + \mathbf{k}_2 - \mathbf{k}} p_{3\mathbf{k}_1 + \mathbf{k}_2 - \mathbf{k}}^\dagger - c_{4\mathbf{k}_1 + \mathbf{k}_2 - \mathbf{k}} p_{4\mathbf{k}_1 + \mathbf{k}_2 - \mathbf{k}}^\dagger \right) \times \right. \\
&\quad \left. \left( c_{1\mathbf{k}_1} p_{1\mathbf{k}_1} + c_{3\mathbf{k}_1} p_{2\mathbf{k}_1} - c_{2\mathbf{k}_1} p_{3\mathbf{k}_1} - c_{4\mathbf{k}_1} p_{4\mathbf{k}_1} \right) \left( c_{1\mathbf{k}_2} p_{1\mathbf{k}_2} + c_{3\mathbf{k}_2} p_{2\mathbf{k}_2} - c_{2\mathbf{k}_2} p_{3\mathbf{k}_2} - c_{4\mathbf{k}_2} p_{4\mathbf{k}_2} \right) \right\} \quad (25)
\end{aligned}$$

$$\begin{aligned}
R_{\mathbf{k}}^{\text{xx},2} &= V_{\text{xx}} \sum_{\mathbf{k}_1, \mathbf{k}_2} B_{2\mathbf{k}_1 + \mathbf{k}_2 - \mathbf{k}}^\dagger B_{2\mathbf{k}_1} B_{2\mathbf{k}_2} \\
&= \frac{V_{\text{xx}}}{2\sqrt{2}} \sum_{\mathbf{k}_1, \mathbf{k}_2} \left\{ \left( c_{1\mathbf{k}_1 + \mathbf{k}_2 - \mathbf{k}} p_{1\mathbf{k}_1 + \mathbf{k}_2 - \mathbf{k}}^\dagger - c_{3\mathbf{k}_1 + \mathbf{k}_2 - \mathbf{k}} p_{2\mathbf{k}_1 + \mathbf{k}_2 - \mathbf{k}}^\dagger - c_{2\mathbf{k}_1 + \mathbf{k}_2 - \mathbf{k}} p_{3\mathbf{k}_1 + \mathbf{k}_2 - \mathbf{k}}^\dagger + c_{4\mathbf{k}_1 + \mathbf{k}_2 - \mathbf{k}} p_{4\mathbf{k}_1 + \mathbf{k}_2 - \mathbf{k}}^\dagger \right) \times \right. \\
&\quad \left. \left( c_{1\mathbf{k}_1} p_{1\mathbf{k}_1} - c_{3\mathbf{k}_1} p_{2\mathbf{k}_1} - c_{2\mathbf{k}_1} p_{3\mathbf{k}_1} + c_{4\mathbf{k}_1} p_{4\mathbf{k}_1} \right) \left( c_{1\mathbf{k}_2} p_{1\mathbf{k}_2} - c_{3\mathbf{k}_2} p_{2\mathbf{k}_2} - c_{2\mathbf{k}_2} p_{3\mathbf{k}_2} + c_{4\mathbf{k}_2} p_{4\mathbf{k}_2} \right) \right\} \quad (26)
\end{aligned}$$

$$\begin{aligned}
R_{\mathbf{k}}^{\text{sat},1} &= \frac{V}{n_{\text{sat}}} \sum_{\mathbf{k}_1, \mathbf{k}_2} B_{1\mathbf{k}_1} a_{1\mathbf{k}_2} B_{1\mathbf{k}_1 + \mathbf{k}_2 - \mathbf{k}}^\dagger \\
&= \frac{V}{2\sqrt{2}n_{\text{sat}}} \sum_{\mathbf{k}_1, \mathbf{k}_2} \left\{ (c_{1\mathbf{k}_1} p_{1\mathbf{k}_1} + c_{3\mathbf{k}_1} p_{2\mathbf{k}_1} - c_{2\mathbf{k}_1} p_{3\mathbf{k}_1} - c_{4\mathbf{k}_1} p_{4\mathbf{k}_1}) (c_{2\mathbf{k}_2} p_{1\mathbf{k}_2} + c_{4\mathbf{k}_2} p_{2\mathbf{k}_2} + c_{1\mathbf{k}_2} p_{3\mathbf{k}_2} + c_{4\mathbf{k}_2} p_{2\mathbf{k}_2}) \times \right. \\
&\quad \left. (c_{1\mathbf{k}_1 + \mathbf{k}_2 - \mathbf{k}} p_{1\mathbf{k}_1 + \mathbf{k}_2 - \mathbf{k}}^\dagger + c_{3\mathbf{k}_1 + \mathbf{k}_2 - \mathbf{k}} p_{2\mathbf{k}_1 + \mathbf{k}_2 - \mathbf{k}}^\dagger - c_{2\mathbf{k}_1 + \mathbf{k}_2 - \mathbf{k}} p_{3\mathbf{k}_1 + \mathbf{k}_2 - \mathbf{k}}^\dagger - c_{4\mathbf{k}_1 + \mathbf{k}_2 - \mathbf{k}} p_{4\mathbf{k}_1 + \mathbf{k}_2 - \mathbf{k}}^\dagger) \right\} \quad (27)
\end{aligned}$$

$$\begin{aligned}
R_{\mathbf{k}}^{\text{sat},2} &= \frac{V}{n_{\text{sat}}} \sum_{\mathbf{k}_1, \mathbf{k}_2} B_{2\mathbf{k}_1} a_{2\mathbf{k}_2} B_{2\mathbf{k}_1 + \mathbf{k}_2 - \mathbf{k}}^\dagger \\
&= \frac{V}{2\sqrt{2}n_{\text{sat}}} \sum_{\mathbf{k}_1, \mathbf{k}_2} \left\{ (c_{1\mathbf{k}_1} p_{1\mathbf{k}_1} - c_{3\mathbf{k}_1} p_{2\mathbf{k}_1} - c_{2\mathbf{k}_1} p_{3\mathbf{k}_1} + c_{4\mathbf{k}_1} p_{4\mathbf{k}_1}) (c_{2\mathbf{k}_2} p_{1\mathbf{k}_2} - c_{4\mathbf{k}_2} p_{2\mathbf{k}_2} + c_{1\mathbf{k}_2} p_{3\mathbf{k}_2} - c_{4\mathbf{k}_2} p_{2\mathbf{k}_2}) \times \right. \\
&\quad \left. (c_{1\mathbf{k}_1 + \mathbf{k}_2 - \mathbf{k}} p_{1\mathbf{k}_1 + \mathbf{k}_2 - \mathbf{k}}^\dagger - c_{3\mathbf{k}_1 + \mathbf{k}_2 - \mathbf{k}} p_{2\mathbf{k}_1 + \mathbf{k}_2 - \mathbf{k}}^\dagger - c_{2\mathbf{k}_1 + \mathbf{k}_2 - \mathbf{k}} p_{3\mathbf{k}_1 + \mathbf{k}_2 - \mathbf{k}}^\dagger + c_{4\mathbf{k}_1 + \mathbf{k}_2 - \mathbf{k}} p_{4\mathbf{k}_1 + \mathbf{k}_2 - \mathbf{k}}^\dagger) \right\}. \quad (28)
\end{aligned}$$



## 7.5. A simple formula for the entanglement of formation

The entanglement of formation,  $E(\rho)$ , is one of the most commonly employed measures of entanglement found in the literature; it quantifies the resources needed to create a given entangled state. This is discussed at length in [21, 20]. For a density matrix  $\rho$ ,  $E(\rho)$  is given by

$$E(\rho) = h \left( \frac{1 + \sqrt{1 - C(\rho)^2}}{2} \right)$$

where  $h$  is the entropy

$$h(x) = -x \log_2 x - (1 - x) \log_2 (1 - x)$$

and

$$C(\rho) = \max \left( 0, \lambda_1 - \sum_{i \geq 2} \lambda_i \right),$$

where  $\lambda_1 > \lambda_2 > \dots > \lambda_n$  are the ordered eigenvalues of the operator

$$\sqrt{\sqrt{\rho} (\sigma_y \otimes \sigma_y) \rho^* (\sigma_y \otimes \sigma_y) \sqrt{\rho}}.$$

Applying the formulae above and equation (14), it is straightforward to show that in the steady state

$$C(\rho) = \begin{cases} 0 & \Delta \leq n \\ \frac{(4\Delta^2 - 1)(n - \Delta)(\Delta + n)}{8\Delta^4 + 2n^2 + \Delta^2(4n(n+3) + 1)} & \text{otherwise} \end{cases}.$$

In order to get a simplified expression for the EOF, we choose to approximate the expression for the binary entropy by the linear function  $h(x) \approx 0.065 + 0.98x$  (which is the best linear fit in the infinity norm), resulting in

$$E(\rho) \approx 0.065 + \frac{0.98 (n^2 - \Delta^2)^2}{(2n^2 + (1 + 12n)\Delta^2 + 8\Delta^4)^2}.$$

This captures the essential dynamics of the EOF as shown in figure 5.

- [1] C. Weisbuch, M. Nishioka, A. Ishikawa, and Y. Arakawa. Observation of the coupled exciton-photon mode splitting in a semiconductor quantum microcavity. *Phys. Rev. Lett.*, 69:3314–3317, Dec 1992.
- [2] A. Armitage, M. S. Skolnick, V. N. Astratov, D. M. Whittaker, G. Panzarini, L. C. Andreani, T. A. Fisher, J. S. Roberts, A. V. Kavokin, M. A. Kaliteevski, and M. R. Vladimirova. Optically induced splitting of bright excitonic states in coupled quantum microcavities. *Phys. Rev. B*, 57(23):14877–14881, Jun 1998.
- [3] Giovanna Panzarini, Lucio Claudio Andreani, A. Armitage, D. Baxter, M. S. Skolnick, V. N. Astratov, J. S. Roberts, Alexey V. Kavokin, Maria R. Vladimirova, and M. A. Kaliteevski. Exciton-light coupling in single and coupled semiconductor microcavities: Polariton dispersion and polarization splitting. *Phys. Rev. B*, 59(7):5082–5089, Feb 1999.

- [4] G. Panzarini, L. C. Andreani, A. Armitage, D. Baxter, M. S. Skolnick, V. N. Astratov, J. S. Roberts, A. V. Kavokin, M. R. Vladimirova, and M. A. Kaliteevski. Cavity-polariton dispersion and polarization splitting in single and coupled semiconductor microcavities. *Physics of Solid State*, 41:1223, 1999.
- [5] G. Panzarini, L. C. Andreani, A. Armitage, D. Baxter, M. S. Skolnick, J. S. Roberts, V. N. Astratov, M. A. Kaliteevski, A. V. Kavokin, and M. R. Vladimirova. Polariton dispersion and polarisation splitting for quantum well excitons in single and coupled microcavities. *Phys. Stat. Sol. a*, 164:91, 1997.
- [6] R. P. Stanley, R. Houdré, U. Oesterle, M. Ilegems, and C. Weisbuch. Coupled semiconductor microcavities. *Appl. Phys. Lett.*, 65:2093, 1994.
- [7] C. Diederichs, J. Tignon, G. Dasbach, C. Ciuti, A. Lemaître, J. Bloch, Ph. Roussignol, and C. Delalande. Parametric oscillation in vertical triple microcavities. *Nature*, 440:904, 2006.
- [8] C. Diederichs, J. Tignon, G. Dasbach, C. Ciuti, A. Lemaître, J. Bloch, Ph. Roussignol, and C. Delalande. Optical parametric oscillation in a vertical triple microcavity. *Superlattices and Microstructures*, 41:301, 2007.
- [9] Carole Diederichs, David Taj, Thimothée Lecomte, Crisitiano Ciuti, Philippe Roussignol, Claude Delalande, Aristide Lemaître, Ludovic Largeau, Olivia Mauguin, Jacqueline Bloch, Charles Leyder, Alberto Bramati, Elisabeth Giacobino, and Jérôme Tignon. Parametric generation of twin photons in vertical triple microcavities. *C. R. Physique*, 8:1198, 2007.
- [10] C. Ciuti. Branch-entangled polariton pairs in planar microcavities and photonic wires. *Phys. Rev. B*, 69(24):245304, Jun 2004.
- [11] D. Pagel, H. Fehske, J. Sperling, and W. Vogel. Strongly entangled light from planar microcavities. *Phys. Rev. A*, 86:052313, Nov 2012.
- [12] S. Portolan, O. Di Stefano, S. Savasta, F. Rossi, and R. Girlanda. Nonequilibrium langevin approach to quantum optics in semiconductor microcavities. *Phys. Rev. B*, 77(3):035433, Jan 2008.
- [13] S. Portolan, O. Di Stefano, S. Savasta, F. Rossi, and R. Girlanda. Dynamics-controlled truncation scheme for quantum optics and nonlinear dynamics in semiconductor microcavities. *Phys. Rev. B*, 77:195305, May 2008.
- [14] C. Ciuti, P. Schwendimann, and A. Quattropani. Theory of polariton parametric interactions in semiconductor microcavities. *Semiconductor Science and Technology*, 18(10):S279, 2003.
- [15] Stefano Portolan and Salvatore Savasta. *Optical Generation and Control of Quantum Coherence in Semiconductor Nanostructures*. Springer, 2010.
- [16] S. Portolan, O. Di Stefano, S. Savasta, and V. Savona. Emergence of entanglement out of a noisy environment: The case of microcavity polaritons. *EPL (Europhysics Letters)*, 88:20003, 2009.
- [17] P.G. Savvidis, J.J. Baumberg, R.M. Stevenson, M.S. Skolnick, D.M. Whittaker, and J.S. Roberts. Angle-resonant stimulated polariton amplifier. *Phys. Rev. Lett.*, 84:1547, 2000.
- [18] P. G. Savvidis, J. J. Baumberg, R. M. Stevenson, M. S. Skolnick, D. M. Whittaker, and J. S. Roberts. Asymmetric angular emission in semiconductor microcavities. *Phys. Rev. B*, 62(20):R13278–R13281, Nov 2000.
- [19] Daniel F. V. James, Paul G. Kwiat, William J. Munro, and Andrew G. White. Measurement of qubits. *Phys. Rev. A*, 64:052312, Oct 2001.
- [20] William K. Wootters. Entanglement of formation of an arbitrary state of two qubits. *Phys. Rev. Lett.*, 80:2245–2248, Mar 1998.
- [21] Scott Hill and William K. Wootters. Entanglement of a pair of quantum bits. *Phys. Rev. Lett.*, 78:5022–5025, Jun 1997.